Coordinated Control of Distributed Energy-Storage Systems for Voltage Regulation in Distribution Networks

Wang, Yu; Tan, K. T.; Peng, Xiao Yang; So, Ping Lam

2015

Wang, Y., Tan, K. T., Peng, X. Y., & So, P. L. (2016). Coordinated Control of Distributed Energy-Storage Systems for Voltage Regulation in Distribution Networks. IEEE Transactions on Power Delivery, 31(3), 1132-1141.

https://hdl.handle.net/10356/84029

https://doi.org/10.1109/TPWRD.2015.2462723

Coordinated Control of Distributed Energy Storage Systems for Voltage Regulation in Distribution Networks

Y. Wang, *Student Member, IEEE*, K. T. Tan, *Member, IEEE*, X. Y. Peng, *Student Member, IEEE*, and P. L. So, *Senior Member, IEEE*

***Abstract*—In this paper, distributed energy storage systems (ESSs) are proposed to solve the voltage rise/drop issues in low-voltage (LV) distribution networks with high penetration of rooftop photovoltaics (PVs). During peak PV generation period, the voltages are mitigated by charging the ESSs, and the stored energy is discharged for voltage support during peak load period. The impact of storage device integrated with PV source on feeder voltages is investigated in detail. A coordinated control method which includes both distributed and localized controls is proposed for distributed ESSs. The distributed control using consensus algorithm regulates the feeder voltages within the required limits, while the localized control regulates the state of charge (SoC) of each ESS within desired SoC range. The entire control structure ensures voltage regulation while effectively utilizes storage capacity under various operation conditions. The proposed control method is evaluated in LV distribution networks and the simulation results validate the effectiveness of this method.**

***Index Terms*—Distributed energy storage systems, coordinated control, voltage regulation, distribution networks.**

I. Introduction

THE penetration of photovoltaics (PVs) into existing distribution networks is rapidly increasing around the world. In Singapore, government has planned to increase PV generation to 350 MWp by 2020 [1]. Except the voltage drop issue caused by peak load demand in distribution networks, the high penetration of PVs will also lead to voltage rise issue during peak PV generation period [2], [3]. So there is a possibility of voltage limits violation during both peak load and peak PV generation periods, which may lead to poor power quality and even equipment failure.

Many techniques have been proposed for voltage regulation in distribution networks. These methods can be employed by the utility grid and its customers. From the utility point of view, the methods include increasing the conductor size [4], installing voltage regulator [5] and changing the set points of secondary transformer tap [6]. However, the fast increasing capacity of PV generation could lead to frequently upgrading of these utility grid facilities, which results in high costs. The other way of solution is by proper control of distributed generation (DG) units at customer end. The methods include curtailing the power of PV generation [7], allowing reactive power compensation of PV inverters [8], [9] and utilizing energy storage systems (ESSs) [10]-[14]. The disadvantage of PV curtailment is that this method reduces the efficiency of PV generation. The R/X ratio in distribution networks is much larger than that in transmission networks, which makes reactive power compensation less effective. As the cost of adding batteries to residential PV systems has continued dropping in recent years, ESSs become a promising solution for voltage regulation in distribution networks [15].

Distributed EESs have been proposed for mitigating voltage rise issue in [10], [11]. In this paper, the idea of using distributed ESSs is pursued for voltage regulation in low-voltage (LV) distribution networks. Thus far, the main challenge is to develop an effective control method to coordinate the operation of distributed ESSs in distribution networks. To mitigate the impacts of rooftop solar PVs, a charging/discharging strategy has been developed in [11] for energy storage devices that are integrated with PV systems. In [12], the reactive capacity of PV inverters combined with a droop-based EES system has been proposed to improve the voltage profiles. These control methods are employed in a decentralized structure, thus the coordination of distributed ESSs is difficult to achieve. If the state of charge (SoC) of an ESS at a particular bus reaches the limits, reactive power compensation or PV power curtailment is inevitable. On the contrary, in [13], the authors have proposed a coordinated control of distributed ESSs with traditional voltage regulators to solve the voltage rise problem. A centralized controller has been developed to broadcast the coordination charging/discharging signal to the distributed SoC controller. In [14], a centralized LV controller has been developed to coordinate inverter-interfaced generators for voltage control. However, the centralized control requires fast and reliable communication links, and the reliability of the control system is highly dependent on the performance of the centralized controller. The distributed control structure which can avoid some drawbacks of centralized and decentralized control is suitable for DG control in smart grid [16]. However, when the distributed control is applied to distributed EESs in

This research work was supported by the School of Electrical and Electronic Engineering, Nanyang Technological University, Singapore, Division of Electrical Engineering, Ngee Ann Polytechnic, Singapore and A*STAR under the Smart Grid Project (SERC Grant No.: 112 120 2022).

distribution networks, further research that considers the actual PV and load profiles, different SoC conditions of ESSs and various topologies of distribution networks still needs to be done.

This paper addresses how to coordinate distributed ESSs in LV distribution networks for voltage regulation. The capacity and SoC of each ESS are taken into account to accommodate daily operation. A coordinated control method which includes both distributed and localized controls is proposed for ESSs. For the distributed control, a consensus algorithm is proposed to regulate the feeder voltages. If the voltages at certain buses violate voltage limits, the consensus algorithm will estimate the power outputs of ESSs to eliminate the voltage violation. For localized control, a SoC control strategy is proposed to regulate the SoC of each ESS. The SoC control avoids depletion or saturation of ESSs for different operation conditions. The entire control method ensures voltage regulation while effectively utilizes all available capacities of ESSs in the system. The ESS is modeled as vanadium redox battery (VRB) whose SoC is estimated for the SoC control. Various case studies are implemented to verify the performance of the proposed method.

The rest of the paper is organized as follows. The description and analysis of voltage rise/drop issues are presented in Section II. In Section III, the VRB model and proposed control method are introduced. Simulation results on a 6-bus distribution feeder are illustrated in detail in Section IV. Section V presents a case study on a 13-bus distribution network. Finally, Section VI gives the conclusion.

II. Problem Description and Analysis

A typical radial distribution feeder with multiple buses as shown in Fig. 1 is used to illustrate the voltage rise/drop issues. Each bus comprises a PV source, an ESS and a local load, which is viewed as a customer. The integration of ESS into PV source forms a dispatchable distributed generation (DG) unit, which is convenient to control for both grid-connected and islanded operations [17].

Generally, the imbalance between PV generation and load demand will cause power flow along the feeder. Depending on the direction and amount of the power flow, voltages along the feeder will rise/drop to some extent. Especially at the end of the feeder, the voltage may exceed the limits during peak PV generation or peak load period. Distribution networks are usually allowed a maximum voltage deviation of 5%-10% (depend on national standards) from the secondary of the transformer to the customer located at the end of the feeder [7]. The method that reduces the power imbalance between PV generation and load demand can mitigate the voltage rise/drop issues. This can be achieved by utilizing distributed ESSs at customer side.

Fig. 2 shows the voltage profiles along radial distribution feeder. The voltage rise along the feeder during peak PV generation period is shown in Fig. 2(a). The voltage drop along the feeder during peak load period is shown in Fig. 2(b).

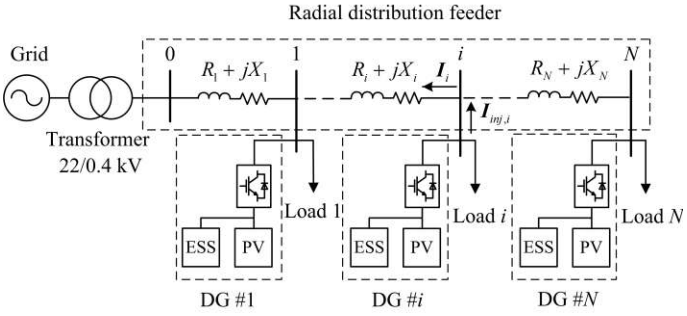

Fig. 1. Radial distribution feeder with multiple buses.

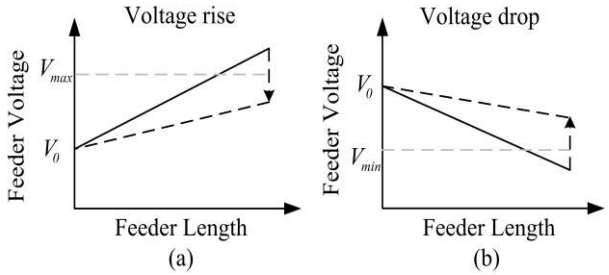

Fig. 2. Voltage profiles along radial distribution feeder. (a) Voltage rise. (b) Voltage drop.

The solid line shows the voltage along the feeder with only PV penetration and the voltage at the end of the feeder exceeds the voltage limits. With proper utilization of ESSs, the power imbalance between PV and load will be reduced. The voltages along the feeder will be regulated to the dashed lines which are within the limits. This problem is further illustrated as follows.

Considering the radial feeder shown in Fig. 1, from the perspective of power injection, the complex power injected at *i*th bus $\boldsymbol{S}_i$ is composed of PV power, ESS power and load power. The voltage relationship and current flow between (*i*-1)th bus and *i*th bus in vector form can be expressed by using power flow analysis as follows:

$$\boldsymbol{S}_i = \boldsymbol{V}_i \boldsymbol{I}_{inj,i}^* \tag{1}$$

$$\boldsymbol{I}_i = \sum_{k=i}^{N} \boldsymbol{I}_{inj,k} = \sum_{k=i}^{N} \frac{\boldsymbol{S}_k^*}{\boldsymbol{V}_k^*} \tag{2}$$

$$\boldsymbol{V}_i = \boldsymbol{V}_{i-1} + \boldsymbol{I}_i (R_i + jX_i) \tag{3}$$

where $\boldsymbol{V}_i$ and $\boldsymbol{V}_i^*$ are the voltage and its conjugate at *i*th bus, $\boldsymbol{I}_{inj,i}$ is the current injected at *i*th bus, $\boldsymbol{I}_i$ and $R_i + jX_i$ are the current and impedance between (*i*-1)th bus and *i*th bus.

The voltage deviation between two adjacent buses can be expressed using the real part in (3) as

$$\Delta V_i = V_i - V_{i-1} = \sum_{k=i}^{N} \frac{P_k \cdot R_k + Q_k \cdot X_k}{V_k} \tag{4}$$

Thus the voltage deviation between the transformer bus V_0 and the last bus V_N can be derived as

$$V_N - V_0 = \sum_{i=1}^{N} \Delta V_i = \sum_{i=1}^{N} \sum_{k=i}^{N} \frac{P_k \cdot R_k + Q_k \cdot X_k}{V_k} \tag{5}$$

where P and Q are the real and reactive power injected at each bus respectively.

According to (4) and (5), both real and reactive power can be utilized to reduce the voltage deviation. However, for typical distribution networks with large R/X ratio, real power is more effective to compensate the voltage deviation compared to reactive power. Large amount of reactive power requires higher power rating inverters and leads to higher losses as well as lower power factors along the LV distribution feeder [18]. In the meanwhile, compared with PV curtailment method proposed in [7], the utilization of ESSs improves the efficiency of PV generation. In this paper, the functions of ESSs are to reduce the real power injection at each bus during the peak PV generation period and reduce the real power absorption at each bus during the peak load demand period. Therefore, the current flow in the distribution feeder will be reduced so that the voltage rise/drop along the feeder can be mitigated.

III. Proposed Control Method

The structure of proposed control method for customer at ith bus is shown in Fig. 3, in which the solid lines show the power flow and the dotted lines show the control signal flow. For each customer, PV panels and storage devices are fed to the dc link through the boost converter and the bidirectional converter respectively. The power is transferred between the dc link and the ac grid through the dc/ac inverter.

As mentioned before, the objective of this paper is to coordinate distributed ESSs for voltage regulation while effectively utilizes the available storage capacity under various operation conditions. The proposed control method includes both distributed and localized control to achieve this goal. As shown in Fig. 3, the distributed control signal utilization ratio u_i is generated by a consensus algorithm which is used to regulate the feeder voltages with distributed ESSs. The localized control signal availability ratio ε_i is provided by SoC control which is used to regulate the SoC of each ESS within the desired SoC range. Finally, the power output of the ESS is determined by multiplying u_i and ε_i with its rated power. A Vanadium redox battery (VRB) model is implemented for grid application, and the SoC is estimated for localized SoC control. The details of the VRB model and the proposed control method are explained in the following subsections.

A. Vanadium Redox Battery

Due to the high efficiency, high scalability, fast response, long time duration and low maintenance requirements, VRB is well suitable for grid-scale applications [19]. In this paper, a residential VRB system rated 5 kW/20 kWh is implemented for energy storage purpose. The VRB is modeled based on the data presented in [19], [20]. The open-circuit voltage (OCV)/SoC characteristic curve of a single VRB cell is shown in Fig. 4. The VRB should be operated in the linear operating region which ranges between 15%-85% of SoC. Each VRB consists of 38 cells connected in series. The parameters for the VRB are shown in Table I.

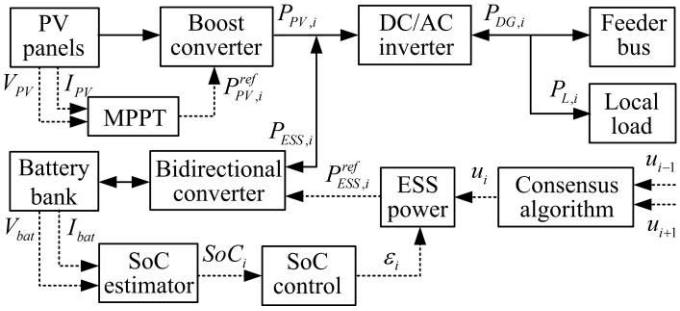

Fig. 3. The structure of proposed control method for customer at ith bus.

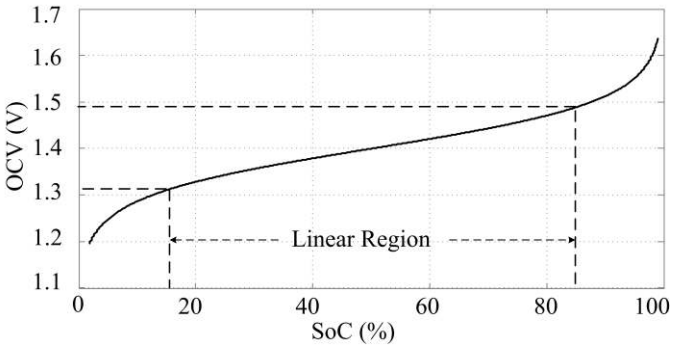

Fig. 4. The OCV/SoC characteristic curve of a single VRB cell.

TABLE I
Parameters of VRB

Cell Configuration	38 Series Cell Stack
Rated Power	5 kW
Rated Capacity	20 kWh
Operation Voltage	42-57 V
SoC Region (SoC^{min}, SoC^{max})	15%, 85%

The SoC of the VRB is calculated using the ampere-hour counting method as follows:

$$SoC(t) = SoC(t-\Delta t) + \Delta SoC \tag{6}$$

$$\Delta SoC = \frac{P_{bat}\Delta t}{C_B} = \frac{V_{bat} I_{bat} \Delta t}{C_B} \tag{7}$$

where C_B is the total energy capacity of the VRB, Δt is the time interval, V_{bat} and I_{bat} are the output voltage and current of the VRB respectively.

B. Distributed Control Method

The first objective of the proposed control method is to coordinate distributed ESSs for voltage regulation. A distributed control using consensus algorithm is applied for ESSs to regulate the feeder voltages within the voltage limits. Consensus algorithm is achieved by sharing variable of interest, called the information state among all available units. The initial information state is determined by the virtual leader which measures the information of the critical point [16], [21]. In this paper, the information state of each ESS is represented by utilization ratio u.

For radial distribution feeder with multiple buses as shown in Fig. 1, the last bus is the critical bus which has the

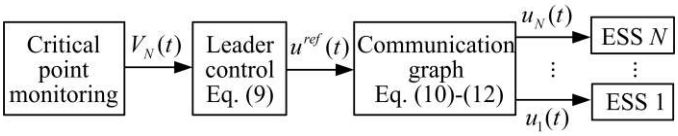

Fig. 5. The control scheme of proposed distributed control.

highest/lowest voltage in the system. Thus the last bus is chosen as the virtual leader to initiate the ESSs coordination. The utilization ratio of the leader is determined by measuring the voltage of the last bus. The utilization ratio of the leader is then shared to available ESSs through communication links to determine the utilization ratio of each ESS to realize the desired voltage regulation objective. The control scheme of proposed distributed control is shown in Fig. 5.

To avoid overvoltage and undervoltage, the voltage upper and lower references (V^{up} and V^{low}) are chosen within the voltage limits (V^{max} and V^{min}) for the consensus algorithm. During both peak PV generation and peak load periods, for arbitrary bus voltage V_i in distribution feeder, the condition given by (8) will be met with the proposed consensus algorithm:

$$V^{low} < V_i(t) < V^{up} \tag{8}$$

The utilization ratio of the leader u^{ref} is updated at discrete time steps. During peak PV generation period, if the voltage of the last bus V_N goes beyond upper voltage reference V^{up}, u^{ref} will be increased. During peak load period, if the voltage of the last bus goes below lower voltage reference V^{low}, u^{ref} will be reduced. During other periods, u^{ref} will be equal to the former value. In general, the utilization ratio of the leader will be updated as follows:

$$u^{ref}(t) = \begin{cases} u^{ref}(t-t_s) + k_1(V_N(t) - V^{up}) & if \quad V_N(t) > V^{up} \\ u^{ref}(t-t_s) & if \quad V^{low} < V_N(t) < V^{up} \\ u^{ref}(t-t_s) + k_2(V_N(t) - V^{low}) & if \quad V_N(t) < V^{low} \end{cases} \tag{9}$$

where V_N is the voltage of the last bus, V^{up} and V^{low} are the upper and lower voltage references respectively. Parameters k_1 and k_2 are the control gains, which affect the convergence speed and control accuracy of the distributed control. t_s is the sampling interval. For daily operation, it should pay attention that the initial value of u^{ref} is 0. u^{ref} will be back to 0 when the control changes from charging mode to discharge mode, and vice versa.

The utilization ratio provided by the leader is then communicated to available ESSs through communication links. The instantaneous communication topology can be represented by the following matrix:

$$S(t) = \begin{bmatrix} s_{11}(t) & s_{12}(t) & \cdots & s_{1N}(t) \\ s_{21}(t) & s_{22}(t) & \cdots & s_{2N}(t) \\ \vdots & \vdots & \ddots & \vdots \\ s_{N1}(t) & s_{N2}(t) & \cdots & s_{NN}(t) \end{bmatrix} \tag{10}$$

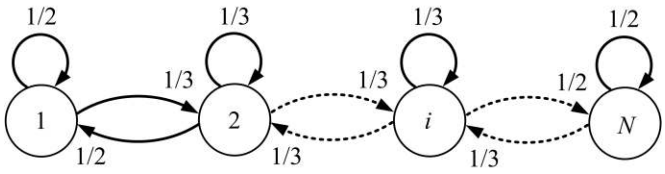

Fig. 6. Communication graph for N-bus radial distribution feeder.

where s_{ij} denotes the communication link between the ith and jth customers. $s_{ii} = 1$ for all i, $s_{ij} = 1$ if the utilization ratio of the jth bus is received by the ith bus at time t, and $s_{ij} = 0$ if otherwise. In this paper, it is assumed that customers can only communicate with their neighbours, which means all $s_{(i)(i-1)} = 1$ and $s_{(i)(i+1)} = 1$ for radial feeder shown in Fig.1.

The utilization ratio for the ith customer is updated as follows:

$$u_i(t) = \sum_{j=1}^{N-1} d_{ij}(t) u_j(t-t_s) + d_{iN}(t) u^{ref}(t-t_s) \tag{11}$$

where $d_{ij}(t)$ is the (i, j) entry of a row stochastic matrix (i.e., row sum of 1) $D(t)$ which can be found in each discrete time data exchange by

$$d_{ij}(t) = \frac{\omega_{ij} s_{ij}(t-t_s)}{\sum_{k=1}^{N} \omega_{ik} s_{ik}(t-t_s)} \tag{12}$$

where the weights ω_{ij} are set to 1 in this paper to share the required real power equally among distributed ESSs and s_{ij} are the entries of communication matrix, given in (10). The ith customer will know the ith row of matrix $D(t)$ to perform the consensus operation. The communication graph for the N-bus radial feeder can be presented using state transitions diagram as shown in Fig. 6.

Although the proposed algorithm is derived under radial distribution feeder with one lateral, it is also applicable for distribution networks with multiple laterals. In such condition, the last bus at each lateral is the critical bus which has the highest/lowest voltage in that lateral. So the last bus of each lateral will be chosen as a virtual leader. If the last bus of this lateral is regulated within the voltage limits, the voltages along this lateral will be within the limits. The utilization ratios of available ESSs are still updated by (11) according to the communication matrices $S(t)$ and $D(t)$. This condition will be further illustrated in Section V.

C. Localized Control Method

The proposed distributed control will regulate the feeder voltages and determine the utilization ratio of each ESS. However, due to different SoCs of ESSs and unpredictable weather/load conditions, the ESSs may get fully charged/discharged when they are needed. The second objective is to effectively utilize the available storage capacity in the network for voltage regulation. Therefore, for each ESS, a localized control based on local SoC information is implemented to adjust the charging/discharging speed.

The localized SoC control proposed in this paper regulates the SoC of each ESS within a desired range of its predefined

reference SoC. The estimated SoC $SoC(t)$ is compared with the reference SoC $SoC^{ref}(t)$ to determine the availability ratio ε. The reference SoC is a function of t, which donates expected SoC change of each ESS during daily operation. For the ESS charging mode of SoC control, ε is defined by the following equation:

$$\varepsilon(t)=\begin{cases} 0 & if \quad SoC(t)-SoC^{ref}(t)\geq a \\ 1-k_3(SoC(t)-SoC^{ref}(t)) & if \quad b<SoC(t)-SoC^{ref}(t)<a \\ 1 & if \quad SoC(t)-SoC^{ref}(t)\leq b \end{cases} \tag{13}$$

where parameters a and b are thresholds of SoC control, which define the allowable SoC deviation range from reference SoC. Parameter k_3 is equal to $1/(a-b)$. If $SoC(t)$ of the ESS is larger than $SoC^{ref}(t)+a$, the availability ratio becomes 0 to stop the charging of the ESS. If $SoC(t)$ of the ESS is within the range $[SoC^{ref}(t)+b,\ SoC^{ref}(t)+a]$, the availability ratio is between 0 and 1 to slow down the charging of the ESS. If $SoC(t)$ of the ESS is smaller than $SoC^{ref}(t)+b$, the availability ratio becomes 1 to make full use of the ESS. The condition for the ESS discharging mode of SoC control is similar, which is not further illustrated here.

Finally, the required power output of ith ESS can be determined by

$$P_{ESS,i}^{ref}(t)=u_i(t)\times\varepsilon_i(t)\times P_{ESS,i}^{rated} \tag{14}$$

$$-1<u_i(t)<1;\ 0<\varepsilon_i(t)<1 \tag{15}$$

where $P_{ESS,i}^{rated}$ is the rated power output of ESS at ith bus.

It is noted that the operation of the ESS should also take into account power and energy constraints. The power limits and SoC limits of the ESS during operation can be described by (16) and (17) respectively

$$-P_{ESS}^{rated}\leq P_{ESS}(t)<P_{ESS}^{rated} \tag{16}$$

$$SoC^{min}<SoC(t)<SoC^{max} \tag{17}$$

When the proposed control method is applied for daily operation, there are several points should be considered. First, based on historical PV and load data, the total storage capacity should be enough to deal with voltage rise/drop issues in the network. Next, although ESSs are installed for voltage regulation purpose, it is expected that the storage capacity is fully used for 24-h operation. Besides, the control method has charging and discharging modes to accommodate daily operation. There will be mode changes at specific time during the operation. Finally, the parameters of the proposed control method should be properly chosen. The upper and lower voltage references define how much power to be charged/discharged by ESSs with distributed control. The reference SoC defines how fast the ESS should be charged/discharged during the operation. In this paper, the upper and lower references are chosen that the ESSs will get fully charged/discharged under normal weather conditions (sunny and cloudy PV profiles in this paper) with only distributed control. The reference SoC, parameters a and b for localized SoC control should cooperate with distributed control, which regulate the power output of the ESS if the SoC exceeds the desired SoC range during the operation. The parameters of the proposed control method are presented in Table II.

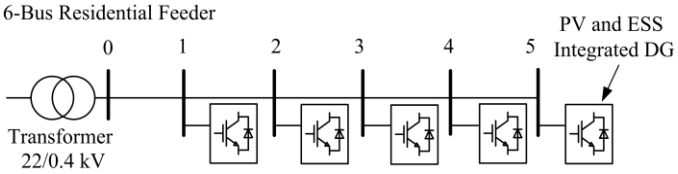

Fig. 7. Single-line diagram of 6-bus test feeder.

TABLE II
PARAMETERS OF PROPOSED CONTROL METHOD

Parameter	Value
Voltage Reference (V^{low}, V^{up})	0.96 p.u., 1.05 p.u.
Distributed Control (k_1, k_2)	0.001, 0.001
SoC Control Charging Mode (a, b, k_3)	0.05, 0, 20
SoC Control Discharging Mode (a', b', k_3')	-0.05, 0, -20

TABLE III
PARAMETERS OF SIMULATION SYSTEM

Feeder Length	500 m
Bus to Bus Distance	100 m
Conductor Size	0.549 + j0.072 Ω/km
MV/LV Transformer Size	100 kVA, 22/0.4 kV
PV Size	9 kWp
VRB Rating	20 kWh/5 kW
Maximum Voltage Deviation	6%

IV. CASE STUDY: 6-BUS DISTRIBUTION FEEDER

In this section, a distribution feeder consisting of six buses is implemented in Matlab/Simulink to investigate the performance of the proposed control method. The residential feeder supplies electricity to five customers by a 100 kVA, 22/0.4 kV transformer. The distance between each bus is 100 m. The single-line diagram of the 6-bus test feeder is shown in Fig. 7. The PV system at the residential households is operated at unity power factor and has the capacity of 9 kWp. A VRB rated at 20 kWh/5 kW is integrated with the rooftop PV system of each customer which is a typical size for residential rooftop PV applications [22]. The voltage at the secondary of the transformer is set at 230 V (1.0 p.u.). This paper allows a maximum 6% voltage deviation in distribution networks. The voltage upper reference (1.05 p.u.) and lower reference (0.96 p.u.) are chosen within this limit. The parameters of the simulation system are presented in Table III.

To test the developed methodology in a realistic environment, two solar PVs output profiles and a residential load profile are used. The PV data is measured using GL130 PV module. It was measured in the summer of the year 2014 at

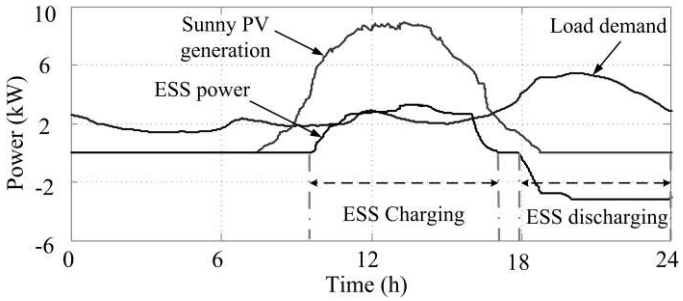

Fig. 8. PV generation, residential load demand and ESS power for test case 1.

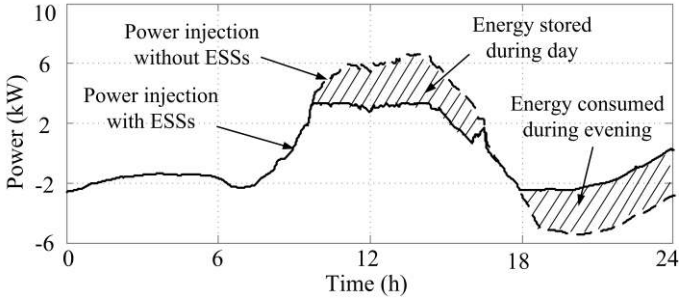

Fig. 9. Power injection with/without ESSs for test case 1.

Clean Energy Research Laboratory, Nanyang Technological University, Singapore. 5-min PV data is used as input data for the PV systems. Customer loads are aggregated into a typical residential load profile, which is presented in [23]. The PV and load data are scaled up for this application. The simulation sampling interval is 0.4 s. To cope with the simulation speed, the PV and load data holds the same value for every 5 minutes. Besides, this study focuses on distribution networks in a community scaled residential area. So it is assumed that customers present identical PV and load profiles in this paper.

A. Test Case 1

The first test case demonstrates the performance of the proposed control method under sunny weather condition with identical initial SoC of each ESS. The initial SoC of each ESS is 20%. The PV power generation, the load demand, the ESS power of the last bus (bus 5) of the radial test feeder is shown in Fig. 8. The corresponding power injection at bus 5 with/without ESSs is shown in Fig. 9. As PV generation, load demand and initial ESS condition is identical for each bus, ESSs at buses 1, 2, 3 and 4 have the same power outputs and SoC profiles as the ESS at bus 5, which are not shown here.

As shown in Figs. 8 and 9, from 8:30 h to 17:10 h, there is more power generated by the PVs than consumed by the loads. Thus the feeder will export real power to the grid which results in voltage rise along the feeder. However, during the other periods, there is no energy produced by PVs so that the load demand is larger than the PV generation. The feeder will import real power from the grid which results in voltage drop. If ESS is installed at each bus, it will start charging at 9:45 h when the voltage at bus 5 exceeds the upper voltage reference (1.05 p.u.). The control changes to discharging mode at 17:00 h. The ESSs will start discharging at 17:50 h when the voltage at bus 5 below the lower voltage reference (0.96 p.u.). In Fig. 9, due to the operation of ESSs at each bus, the power

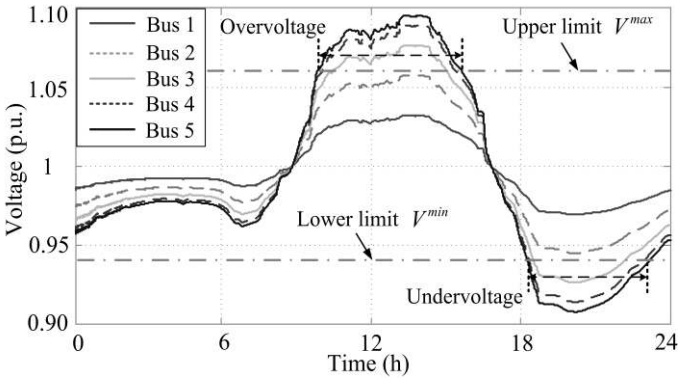

Fig. 10. 24-h voltage profiles without ESSs for a sunny day.

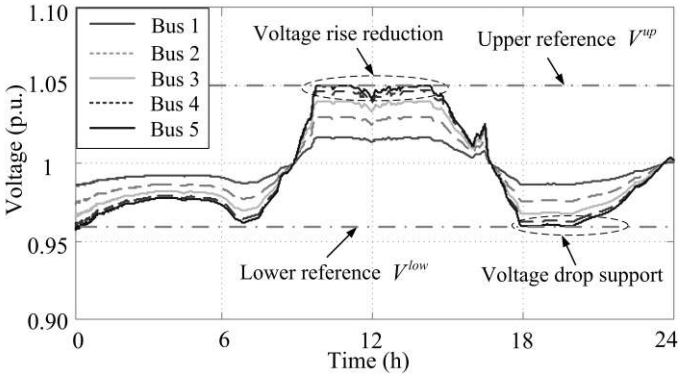

Fig. 11. 24-h voltage profiles with ESSs and proposed method for a sunny day.

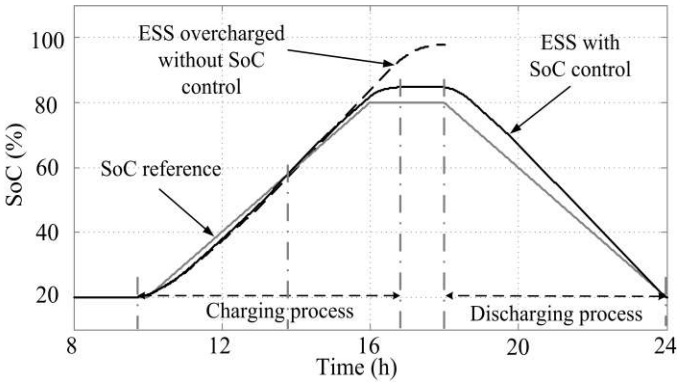

Fig. 12. SoC profiles for test case 1.

injection/absorption at bus 5 with ESSs (solid line) is smaller than the power without ESSs (dotted line). The energy stored during the daytime is utilized for voltage support during the evening.

Figs. 10 and 11 present the corresponding voltage profiles of each bus without and with ESSs respectively. In Fig. 10, the maximum voltage (1.093 p.u.) occurs at noon and the minimum voltage (0.912 p.u.) occurs at evening both in bus 5. The voltage exceeds the upper voltage limit (1.06 p.u.) from 10:00 h to 15:45 h. Buses 3, 4 and 5 experience overvoltage for at least a small period of time during the daytime. The voltage drops below the lower voltage limit (0.94 p.u.) from 18:20 h to 23:00 h. Buses 3, 4 and 5 experience undervoltage for at least a small period of time during the evening. As shown in Fig. 11, with ESSs installed at each bus and proposed control method, the voltage is regulated below V^{up} (1.05 p.u.) for overvoltage period, and the voltage is regulated above V^{low}

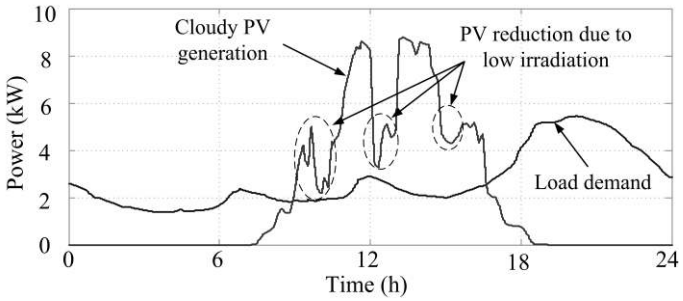

Fig. 13. PV generation and residential load demand for test case 2.

(0.96 p.u.) for undervoltage period.

The corresponding SoC profiles of the ESS at bus 5 are shown in Fig. 12. The SoC changing speed is corresponding to the power output of the ESS. The SoC reference curve used in this test case for the SoC control is also shown in Fig. 12. As shown in Fig. 12, the SoC increases to 84.5% at the end of charging process and reduces to 19.8% at the end of discharging process. At the first part of charging process, the SoC profile is lower than the SoC reference, which means the ESS is fully available during this period and the availability ratio ε=1. At the second part of the charging process, the SoC profile is higher than the SoC reference, which means that the ESS is partly available and the availability ratio ε is between 0 and 1 to restrict the overcharging of the ESS. During most time of discharging process, the ESS is fully available for discharging. It is also seen from Fig. 12 that the SoC profile without the SoC control (dotted line) will exceed the SoC operation range of the VRB at the end of charging process.

B. Test Case 2

The second test case further demonstrates the performance of the proposed control method under cloudy weather condition with different initial SoC of each ESS. In this test case, the initial SoCs of ESSs at buses 1, 2, 3, 4 and 5 are 50%, 35%, 30%, 25% and 20% respectively. ESS at bus 1 is plugged out at 12:00 h, and plugged back into the feeder at 13:00 h. Fig. 13 shows the PV output and the load demand in this condition. In Fig. 13, as there are several large variations of solar irradiation during the daytime, the total PV generation is smaller than in test case 1.

Figs. 14 and 15 present the voltage profiles of each bus without and with ESSs respectively in test case 2. In Fig. 14, due to the variations of solar irradiation, overvoltage time is from 10:50 h to 12:10 h and 13:05 h to 14:45 h, which is shorter than in Fig. 10. Buses 3, 4, and 5 still experience overvoltage and undervoltage for some period of time. As shown in Fig. 15, with ESSs installed at each bus and proposed control method, voltages along the feeder are regulated within the voltage references.

The corresponding power outputs and SoC profiles of ESSs are shown in Figs. 16 and 17 respectively. The time sequences of the operation are explained as follows:

1) At 10:50 h, the voltage of bus 5 exceeds the upper voltage reference. ESSs 2, 3, 4, and 5 start to charge while the power output of ESS 1 remains 0 until 11:30 h. The reason is that the initial SoC of ESS 1 is 50%, which is out of the desired SoC range (larger than ($SoC^{ref}(t)$+0.05)) of SoC control. The availability ratio ε of ESS1 keeps 0 to prevent the charging of ESS1.
2) From 11:30 h to 12:00 h, the charging power of ESS 1 is smaller than the charging power of ESSs 2, 3, 4, and 5. The availability ratio ε of ESS 1 is between 0 and 1 but still smaller than 1.

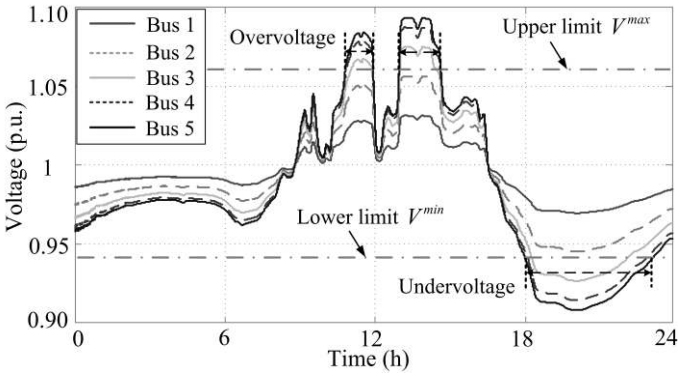

Fig. 14. 24-h voltage profiles without ESSs for a cloudy day.

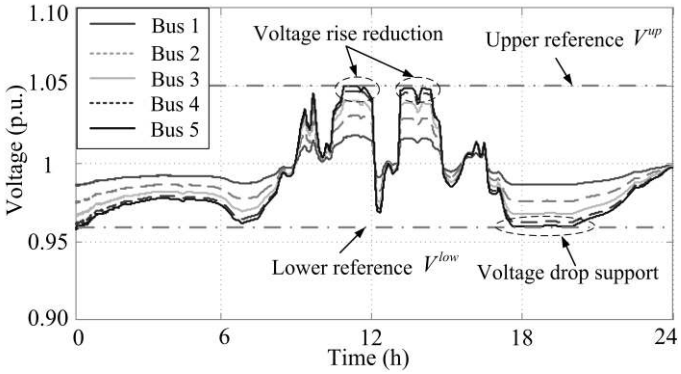

Fig. 15. 24-h voltage profiles with ESSs and proposed method for a cloudy day.

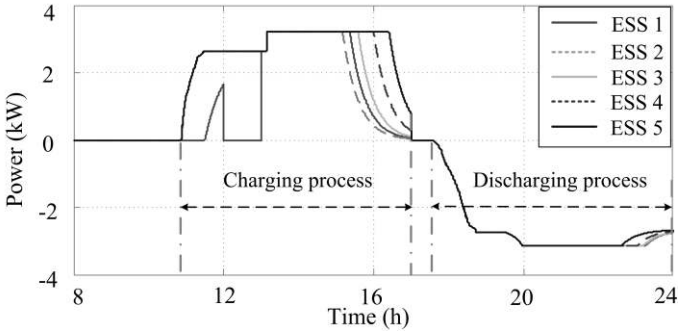

Fig. 16. Power outputs of ESSs for test case 2

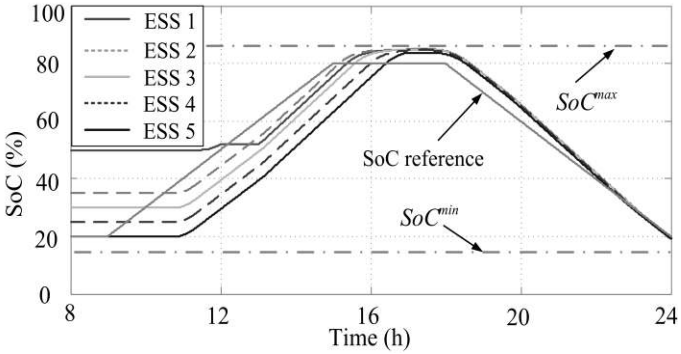

Fig. 17. SoC profiles of ESSs for test case 2.

3) From 12:00 h to 13:00 h, ESS 1 is plugged out while ESSs 2, 3, 4 and 5 are still operated normally in the distribution feeder. The SoC of ESS 1 keeps the same value for an hour.
4) From 13:00 h to 15:10 h, all ESSs are fully available (ε=1) for distributed control.
5) From 15:10 h to 17:00 h, the charging speed of each ESS starts to slow down. The availability ratio ε of each ESS drops between 0 and 1 to reduce the charging power of each ESS.
6) At 17:00 h, the SoC control changes from changing mode to discharging mode.
7) From 17:00 h to 24:00 h, each ESS starts to discharge when the voltage of bus 5 drops below lower voltage reference at 17:50 h. The SoC of each ESS reduces during the discharging process.

C. Comparison with Droop Based Method

In this part, a comparison with droop based method proposed in [7] and [11] is made to further illustrate the features of the proposed method. The droop based method is a typical voltage regulation method which was first applied to curtail PV power in [7] and then applied in [11] to achieve decentralized control of distributed ESSs. This method uses local voltage to define how much power should be curtailed from PV inverters or stored in ESSs. The comparison is implemented with the same condition as in Test Case 1. Fig. 18 shows the voltage profiles with droop based method. Fig. 19 shows the power curtailed with constant droop based method during the daytime. As shown in Fig. 19, the PV energy curtailed at buses 3, 4 and 5 are about 7 kWh, 18.1 kWh and 23.3 kWh respectively. While the total energy generation for the sunny PV condition is about 58.6 kWh. This means that 11.9%, 30.9% and 39.8% of total PV production are curtailed at buses 3, 4 and 5 respectively.

Even though the curtailed energy can be stored in ESSs as proposed in [11], there are still several limitations of this method. ESSs are usually randomly deployed in the system other than well planned. However, as shown in Fig. 19, the requirement of storage capacity with constant droop method increases along the feeder. In the meanwhile, variable droop method allows random deployment of ESSs, but this method requires specific calculation of droop parameters according to system condition. In practical situation, parameters of the system are always changing. Real-time estimation of droop parameters make this method difficult to realize. Besides, ESSs in distribution networks usually have plug and play ability, which leads to different SoC of each ESS. The ESS at certain bus may be fully charged/discharged when it is needed. In order to regulate voltage at this particular bus, PV curtailment and reactive compensation is inevitable. Compared with droop based method, the proposed method allows arbitrary deployment of distributed ESSs as long as the total storage capacity is enough for voltage regulation. All available storage capacity in the system can be effectively utilized for voltage regulation.

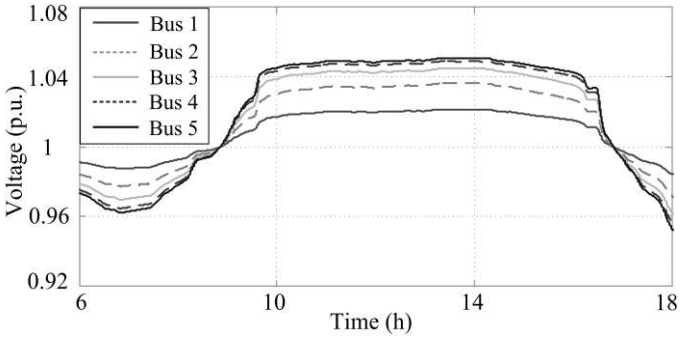

Fig. 18. Voltage profiles with droop based method.

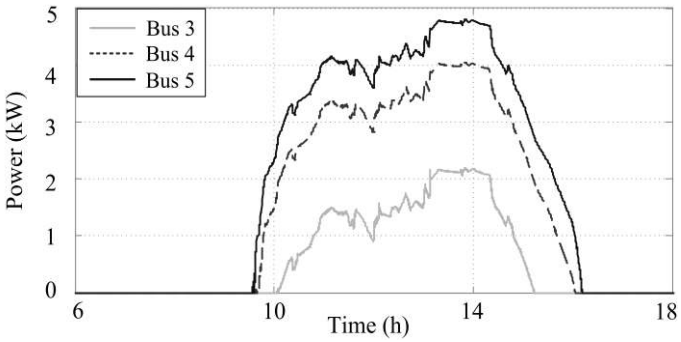

Fig. 19. Power curtailed with constant droop based method.

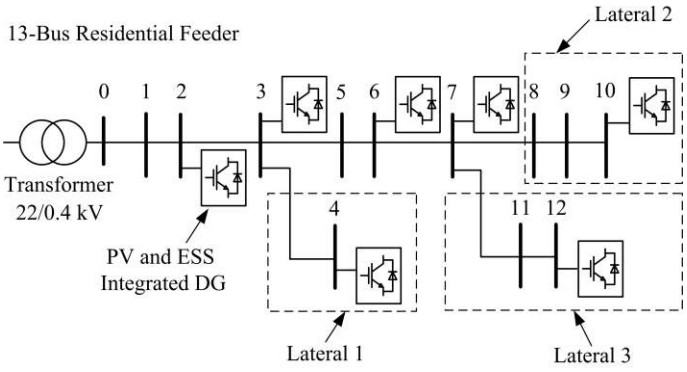

Fig. 20. Configuration of the 13-bus residential distribution network.

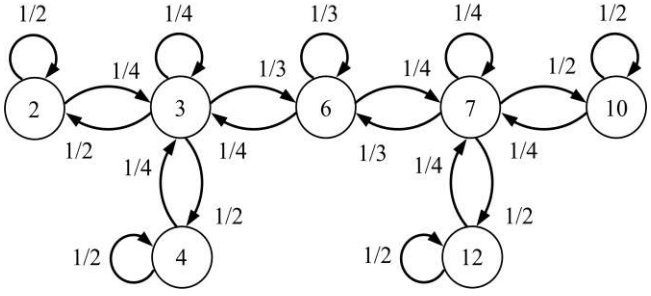

Fig. 21. Communication graph for the 13-bus distribution feeder.

V. Case Study: 13-Bus Distribution Network

In this section, the performance of the proposed control method is demonstrated in a residential distribution network with multiple laterals. The configuration of the test system is a 13-bus distribution network which is a part of IEEE 34-bus system [24] as shown in Fig. 20. The residential feeder supplies electricity to twelve customers by a 22/0.4kV transformer, with seven households installed PV and storage

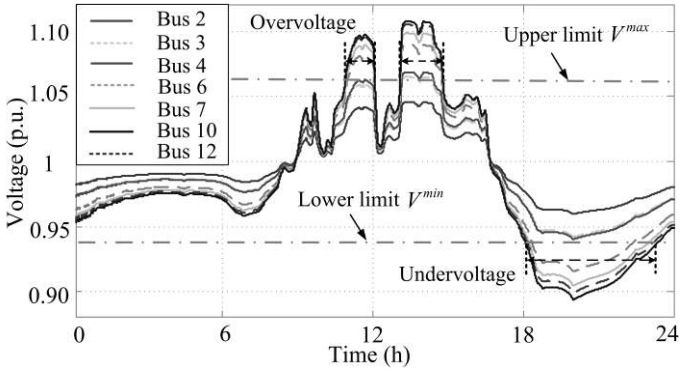

Fig. 22. 24-h voltage profiles without ESSs.

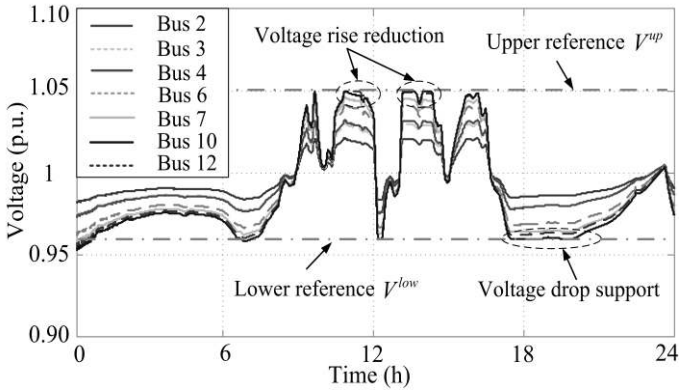

Fig. 23. 24-h voltage profiles with ESSs and proposed method.

integrated DG units. The distance between each bus is 50m. The PV profile is the same as that in Fig. 13. The load demand profile is 50% of that in Fig. 13. The initial SoCs of ESSs at buses 2, 3, 6 and 7 are 20%, and the initial SoCs of ESSs at buses 4, 10 and 12 are 30%, 40% and 50% respectively.

As shown in Fig. 20, the distribution network has three laterals. Buses 4, 10 and 12 are at the end of each lateral and have the highest/lowest voltage in each lateral. So they are chosen as virtual leaders for distributed control. It is also assumed that each bus can communicate with its adjacent buses. The communication graph for the 13-bus distribution network is presented using state transitions diagram as shown in Fig. 21. Figs. 22 and 23 show the voltage profiles of each bus without and with ESSs respectively in this case study. In Fig. 22, the overvoltage and undervoltage are even severe than in Fig. 14. The voltages at most bus will violate the voltage limits during peak PV generation/load periods. Bus 10 has the longest distance to the secondary of the transformer, so the voltage at bus 10 is the highest/lowest in the network. As shown in Fig. 23, with the proposed control method adopted by ESSs, voltages in the network are regulated within the voltage references.

The corresponding power outputs and SoC profiles of ESSs are shown in Figs. 24 and 25 respectively. ESSs 2, 3, 6 and 7 have the same power outputs and SoC profiles, so only the profiles of ESS 7 are shown here. The time sequences of the operation are detailed as follows:

1) At 9:30 h, ESSs 2, 3, 6 and 7 start to charge. The power output of ESS 10 remains 0 until 10:30 h and the power output of ESS 12 remains 0 until 11:30 h.

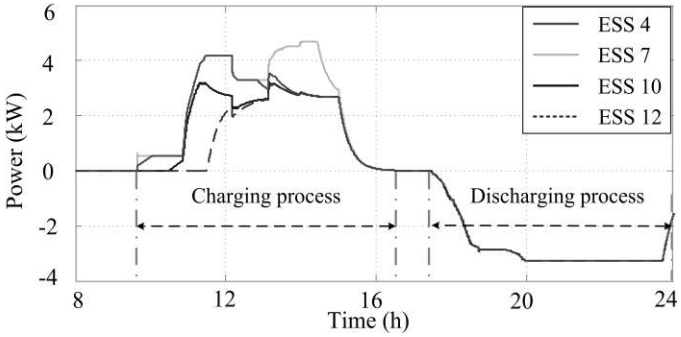

Fig. 24. Power outputs of ESSs 4, 7, 10 and 12.

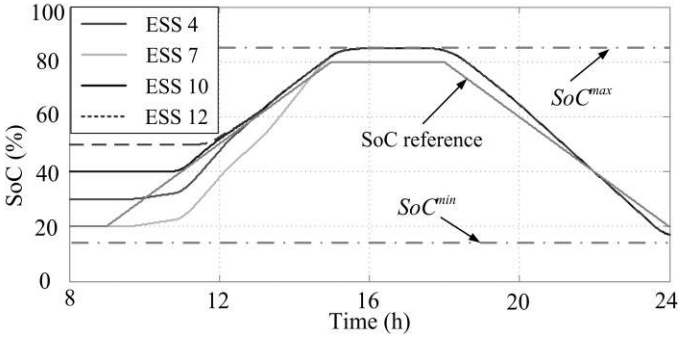

Fig. 25. SoC profiles of ESSs 4, 7, 10 and 12.

2) At 12:10 h, due to the large variation of solar irradiation, there is a sudden drop of charging power of each ESS.
3) From 13:10 h to 15:30 h, ESSs 2, 3, 6 and 7 have more charging power than ESSs 4, 10 and 12.
4) From 15:30 h to 17:00 h, the charging speed of each ESS slows down quickly.
5) At 17:00 h, the SoC control changes from changing mode to discharging mode.
6) From 17:00 h to 24:00 h, each ESS starts to discharge at 17:30 h. The SoC of each ESS reduces during the discharging process.

VI. Conclusion

In this paper, distributed ESSs have been utilized to regulate the voltages in LV distribution networks with high PV penetration. The impact of ESS integrated with PV source on feeder voltages has been investigated. A coordinated control method has been proposed for voltage regulation while effectively utilizing storage capacities of ESSs during daily operation. The power outputs of ESSs are determined by both distributed control and localized SoC control. Real-time SoC of each ESS is estimated for the proposed control method.

A simulation platform has been implemented in Matlab/Simulink to validate the performance of the proposed control method under various operation conditions. The simulation results have demonstrated that the proposed control method ensures the voltages in the networks within the voltage limits during the daily operation. Based on the SoC condition of each ESS, the power sharing among each ESS for voltage regulation is automatically determined. So the SoC of each ESS is regulated within desired SoC range during the

operation. Besides, the proposed method can be implemented to distribution networks with multiple laterals.

REFERENCES

[1] [Online]. Available: https://www.ema.gov.sg/Solar_Photovoltaic_ Systems.aspx.

[2] C. W. Brice, "Voltage-drop calculations and power-flow studies for rural electric distribution lines," *IEEE Trans. Industry Applications*, vol. 28, no. 4, pp. 774-781, Jul./Aug. 1992.

[3] R. Tonkoski, D. Turcotte, and T. H. M. El-Fouly, "Impact of high PV penetration on voltage profiles in residential neighborhoods," *IEEE Trans. Sustainable Energy*, vol. 3, no. 3, pp. 518-527, Jul. 2012.

[4] C. L. Masters, "Voltage rise: The big issue when connecting embedded generation to long 11kV overhead lines," *Power Engineering Journal*, vol. 16, pp. 5-12, 2002.

[5] M. E. Elkhatib, R. El Shatshat, and M. M. A. Salama, "Optimal control of voltage regulators for multiple feeders," *IEEE Trans. Power Delivery*, vol. 25, no. 4, pp. 2670-2675, Oct. 2010.

[6] M. Todorovski, "Transformer voltage regulation−compact expression dependent on tap position and primary/secondary voltage," *IEEE Trans. Power Delivery*, vol. 29, no. 3, pp. 1516-1517, Apr. 2014.

[7] R. Tonkoski, L. A. C. Lopes, and T. H. M. El-Fouly, "Coordinated active power curtailment of grid connected PV inverters for overvoltage prevention," *IEEE Trans. Sustainable Energy*, vol. 2, no. 2, pp. 139-147, Apr. 2011.

[8] A. Samadi, R. Eriksson, L. Söder, B. G. Rawn, et. al., "Coordinated active power-dependent voltage regulation in distribution grids with PV systems," *IEEE Trans. Power Delivery*, vol. 29, no. 3, pp. 1454-1464, Jan. 2014.

[9] P. Jahangiri and D. C. Aliprantis, "Distributed volt/var control by PV inverters," *IEEE Trans. Power Systems*, vol. 28, no. 3, pp. 3429-3439, Aug. 2013.

[10] M. J. E. Alam, K. M. Muttaqi, and D. Sutanto, "Distributed energy storage for mitigation of voltage-rise impact caused by rooftop solar PV," *IEEE Power and Energy Society General Meeting*, *2012*, pp. 1-8, Jul. 2012.

[11] M. J. E. Alam, K. M. Muttaqi, and D. Sutanto, "Mitigation of rooftop solar PV impacts and evening peak support by managing available capacity of distributed energy storage systems," *IEEE Trans. Sustainable Energy*, vol. 28, no. 4, pp. 3874-3884, May 2013.

[12] M. N. Kabir, Y. Mishra, G. Ledwich, Z. Y. Dong, et. al., "Coordinated control of grid-connected photovoltaic reactive power and battery energy storage systems to improve the voltage profile of a residential distribution feeder," *IEEE Trans. Industrial Informatics*, vol. 10, no. 2, pp. 967-977, Jan. 2014.

[13] X. H. Liu, A. Aichhorn, L. M. Liu, and H. Liu, "Coordinated control of distributed energy storage system with tap changer transformers for voltage rise mitigation under high photovoltaic penetration," *IEEE Trans. Smart Grid*, vol. 3, no. 2, pp. 897-906, Feb. 2012.

[14] R. Caldon, M. Coppo, and R. Turri, "Distributed voltage control strategy for LV networks with inverter-interfaced generators," *Electric Power Systems Research*, vol. 107, pp. 85-92, Feb. 2014.

[15] New York State Research and Development Authority. *Residential Solar Energy Storage Analysis*. Prepared by DNV KEMA. Albany, NY: NYSERDA, 2013.

[16] A. Maknouninejad and Q. Zhihua, "Realizing unified microgrid voltage profile and loss minimization: a cooperative distributed optimization and control approach," *IEEE Trans. Smart Grid*, vol. 5, no. 4, pp. 1621-1630, Apr. 2014.

[17] M. B. Delghavi and A. Yazdani, "A unified control strategy for electronically interfaced distributed energy resources," *IEEE Trans. Power Delivery*, vol. 27, no. 2, pp. 803-812, Feb. 2012.

[18] F. Viawan and A. Sannino, "Voltage control with distributed generation and its impact on losses in LV distribution systems," *IEEE Power Tech*, Russia, 2005, pp.1-7.

[19] Q. Xin, T. A. Nguyen, J. D. Guggenberger, M. L. Crow, and A. C. Elmore, "A field validated model of a vanadium redox flow battery for microgrids" *IEEE Trans. Smart Grid*, vol. 5, no. 4, pp. 1592-1601, Jul. 2014.

[20] L. Barote, C. Marinescu, and M. Georgescu, "VRB modeling for storage in stand-alone wind energy systems," *IEEE PowerTech*, Bucharest, 2009, pp. 1-6.

[21] G. Mokhtari, A. Ghosh, G. Nourbakhsh, and G. Ledwich, "Smart robust resources control in LV network to deal with voltage rise issue," *IEEE Trans. Sustainable Energy*, vol. 4, no. 4, pp. 1043-1050, Oct. 2013.

[22] Y. Ru, J. Kleissl, and S. Martinez, "Storage size determination for grid-connected photovoltaic systems," *IEEE Trans. Sustainable Energy*, vol. 4, no. 1, pp. 68-81, Jan. 2013.

[23] A. J. Jardini, Carlos M. V. Tahan, M. R. Gouvea, S. U. Ahn, et. al., "Daily load profiles for residential, commercial and industrial low voltage consumers," *IEEE Trans. Power Delivery*, vol. 15, no. 1, pp. 375-380, Jan. 2000.

[24] IEEE PES, Distribution Test Feeders, Sep. 2010. [Online]. Available: http://www. ewh.ieee.org/soc/pes/dsacom/testfeeders/.

Y. Wang (S'12) received the B.Eng. degree in Electrical and Electronic Engineering from Wuhan University, China, in 2011 and the M.Sc. degree in Power Engineering from Nanyang Technological University, Singapore, in 2012. He is currently working towards the Ph.D. degree in Interdisciplinary Graduate School, Nanyang Technological University, Singapore. His research interests include renewable energy sources, energy storage systems, and smart grids.

K. T. Tan (M'14) received the B.Eng. and Ph.D. degrees in Electrical and Electronic Engineering from Nanyang Technological University, Singapore, in 2008 and 2014 respectively. He then joined the School of Electrical and Electronic Engineering, Nanyang Technological University, Singapore as a Research Engineer and subsequently as a Research Fellow. He is currently a Lecturer in the School of Engineering, Division of Electrical Engineering, Ngee Ann Polytechnic, Singapore. His research interests include clean and renewable energy, microgrids, smart grids, and electric vehicles.

X. Y. Peng (S'11) received the B.Eng. degree in Electrical and Electronic Engineering from Wuhan University, China, in 2010 and the M.Sc. degree in Power Engineering from Nanyang Technological University, Singapore, in 2011. He is currently working towards the Ph.D. degree in the Clean Energy Research Laboratory, School of Electrical and Electronic Engineering, Nanyang Technological University. His research interests include smart grids, control strategy in microgrids, and distributed energy resources.

P. L. So (M'98–SM'03) received the B.Eng. degree with first class honors in Electrical Engineering from the University of Warwick, U.K., in 1993 and the Ph.D. degree in Electrical Power Systems from Imperial College, University of London, U.K., in 1997. He is currently an Associate Professor in the School of Electrical and Electronic Engineering, Nanyang Technological University, Singapore. Prior to his academic career, he worked for 11 years as a Second Engineer with China Light and Power Company Limited, Hong Kong, in the field of power system protection. His research interests include power system stability and control, power quality, power line communications, clean and renewable energy, energy management, microgrids and smart grids. Dr. So was the Chair of the IEEE Singapore Section from 2009 to 2010.